Bulletin of the Seismological Society of America, Vol. 104, No. 2, pp. 624–633, April 2014, doi: 10.1785/0120130024

Ground-Motion Attenuation and Source Spectral Shape for Earthquakes in Eastern Iran

by Aghdas Meghdadi and Jafar Shoja-Taheri

Abstract We study source, path, and site effects for eastern Iran earthquake, based on regression analysis of 243 three-component Fourier acceleration spectra from 32 eastern Iran earthquakes with moment magnitude **M** 4.4–7.4, recorded at hypocentral distances from 5 to 250 km. The geometric spreading follows a trilinear behavior. The first and second hinges of the trilinear behavior are at 87 and 119 km, respectively. The associated quality factor (Q) based on the horizontal components is $Q(f) = 166f^{1.13}$. The site-dependent parameters κ_0 for vertical and horizontal components are 0.035 and 0.048, respectively. Because of lack of station-specific site information, the horizontal-to-vertical ratio is considered to be a rough estimation of generic site amplification. The mean value of Brune stress drops estimated for the events is 81 bars. To construct an empirical model for source spectra (horizontal component of the shear-wave spectrum), for **M** 4.4–7.4, we tested several functional forms, including those suggested for California and eastern North America, to search for the best combination of the coefficients that minimizes the average residual errors. The model we attained is a function of two multiplicative corner frequencies of f_a and f_b and a parameter ε: $A_0(f, M_0) = CM_0(2\pi f)^2/\{[1 + (f/f_a)^2]^{\varepsilon}[1 + (f/f_b)^2]^{1-\varepsilon}\}$, in which $\log(f_a) = 2.69 - 0.56\mathbf{M}$, $\log(f_b) = 3.40 - 0.53\mathbf{M}$, and $\log(\varepsilon) = 0.10 - 0.03\mathbf{M}$.

Introduction

The eastern part of Iran is a region with high levels of seismic activity and has suffered numerous destructive earthquakes with thousands of casualties throughout its long history, including several major ones in recent decades (e.g., 1968 **M** 7.4 Dasht-e-Bayaz, 1978 **M** 7.4 Tabas, 1979 **M** 7.0 Ghaen, 1979 **M** 7.2 Birjand, 1981 **M** 7.2 Sirch, 2003 **M** 6.6 Bam, etc.). The major tectonic provinces of the region are the Kopet Dagh folded belt (Tchalenko, 1975), eastern Albourz, and eastern Iran's plateau, an area of complex block movement. Near its southwest corner, the region approaches the Zagros main thrust line. Along its eastern edge, the region is bound by the north–south trending Harirood fault which, despite its current aseismic character and pre-Jurassic age (Stöcklin, 1968), serves as a boundary between the aseismic zone of western Afghanistan and the highly seismic region of eastern Iran (Shoja-Taheri and Niazi, 1981).

A reliable seismic-hazard evaluation for this region requires the study of the regional specific seismic-source and wave-propagation parameters. These parameters can be used to predict average expected ground-motion amplitudes. The result of analyses of strong ground motion records are used to examine the key specific characteristics of seismic source and seismic propagation of ground motions (e.g., geometrical spreading coefficient, anelastic attenuation coefficient that is inversely related to the quality factor Q, the spectral decay parameter kappa κ described in the following sections). Source spectral amplitudes $A_0(M_0, f)$ of earthquakes are evaluated by correcting the Fourier acceleration amplitude for wave-propagation parameters. We also estimate a model of two-corner source spectra for eastern Iran based on works of Boatwright and Choy (1992), Atkinson (1993), Haddon (1996), and Joyner (1997). This model is compared with similar two-corner source models evaluated for other regions and with the one-corner frequency of the Brune (1970) model.

Strong Ground Motion Data

In this study, Fourier amplitude spectra of 729 acceleration time series, with 200 samples per sec recorded by 243 three-component of instruments obtained from the Iran Strong Motion Network (ISMN) (see Data and Resources) for 32 earthquakes (see Fig. 1 and Table 1), were computed and analyzed. The earthquake moment magnitudes are between 4.4 and 7.4 with hypocentral distances between 5 and 250 km. Figure 2 shows distribution of magnitudes versus distances. Moment magnitudes were obtained from the Global Centroid Moment Tensor (CMT) catalog (see Data and Resources section) for the events with $\mathbf{M} \geq 5.0$.

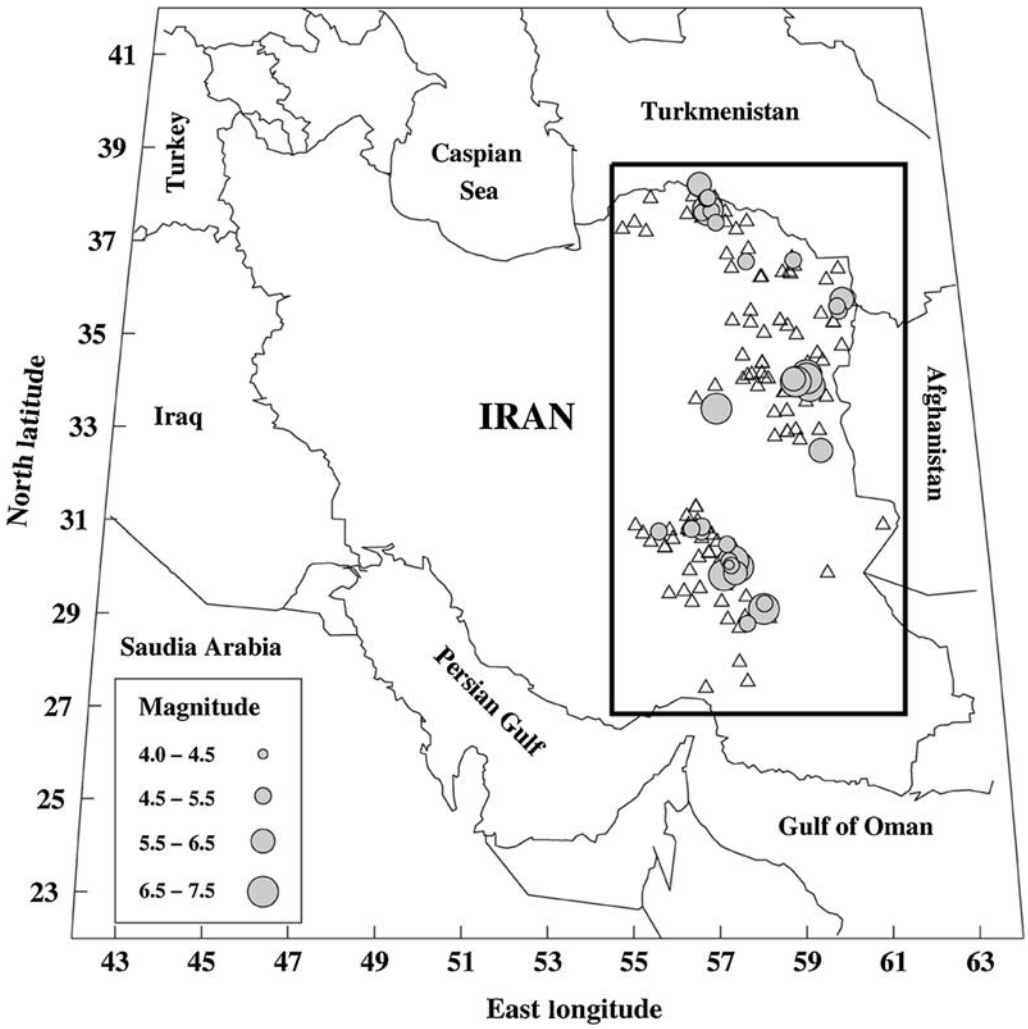

Figure 1. Distribution of earthquakes in eastern Iran that were used in this study. Triangles display locations of the recording stations.

Magnitudes of smaller events were determined by using strong-motion data.

Attenuation of Ground-Motion Amplitudes

Empirical studies of the attenuation of ground-motion amplitudes are usually based on regression of data to a relation of the form

$$\log A_{ij}(f) = \log A_{i0}(f) - b \log R_{ij} - c_4(f) R_{ij} + \log S_j(f), \quad (1)$$

in which $A_{ij}(f)$ is the observed spectral amplitude of earthquake i at station j, $A_{i0}(f)$ is the source spectral amplitude of earthquake i, R_{ij} is the hypocentral distance, b is the coefficient of geometrical spreading, $c_4(f)$ is the coefficient of anelastic attenuation, and $S_j(f)$ corresponds to site response (e.g., Atkinson, 1989; Woodgold, 1990; Atkinson and Mereu, 1992). These coefficients are discussed in the following sections.

Site Effect $S(f)$

It is well known that the soil layers at a given site influence the final surface ground motion and cause modification of amplitude and frequency content of the bedrock motion. Although this modification is a part of the path effect, local site conditions are considered to be independent of the distance between the source and the site. In general, the overall site effect $S(f)$ is the site amplification at near surface $B(f)$ multiplied by the near-surface attenuation, which is commonly used as $\exp(\pi f \kappa_0)$ (Boore and Joyner, 1997; Boore, 2003):

$$S(f) = B(f) e^{-\pi f \kappa_0}. \quad (2)$$

Because of the lack of adequate information on soil classification for the ISMN stations used in this study, we can alternatively replace the site amplification $B(f)$ with the horizontal-to-vertical (H/V) ratio, which is generally known to be a rough estimate of site amplification (e.g., Nakamura, 1989; Lermo and Chávez-García, 1993; Beresnev and

Table 1
Information on the Eastern Iran Earthquakes Used in This Study

Number	Date (yyyy/mm/dd)	Time (UTC)	Longitude E (°)	Latitude N (°)	Depth (km)	M	Number of Recording Stations	Δσ (bar)*	f_0 (Hz)†
1	1978/09/16	15:35:57	57.43	33.38	10	7.4	9	108	0.07
2	1979/01/16	09:50:00	59.52	33.96	10	6.5	12	135	0.22
3	1979/11/14	02:21:18	59.81	34.03	3	6.5	10	99	0.20
4	1979/11/27	17:10:33	59.81	34.10	9	7.0	14	134	0.12
5	1981/06/11	07:24:25	57.42	29.81	20	6.6	2	82	0.17
6	1981/07/28	17:22:23	57.78	29.99	14	7.2	7	75	0.08
7	1989/11/20	04:19:05	57.71	29.86	16	5.9	3	54	0.33
8	1997/02/04	09:53:55	57.33	37.59	10	5.4	6	142	0.80
9	1997/02/04	10:37:47	57.49	37.65	9	6.5	14	94	0.20
10	1997/02/05	07:53:45	57.58	37.63	4	5.2	4	96	0.88
11	1997/05/10	07:57:29	59.87	33.86	9	7.2	27	50	0.07
12	1997/06/25	19:38:40	59.47	34.01	20	5.8	12	118	0.47
13	1998/03/14	19:40:27	57.67	30.11	16	6.6	7	52	0.14
14	1998/04/10	15:00:53	60.03	32.48	8	5.7	4	142	0.56
15	1998/04/16	07:47:10	57.57	30.12	10	4.9	3	27	0.81
16	1998/11/18	07:39:23	57.53	30.47	16	5.3	6	53	0.64
17	1999/01/02	03:28:02	57.61	30.02	2	4.6	3	155	2.06
18	1999/11/08	21:37:23	60.90	35.73	10	5.5	3	88	0.60
19	2000/08/22	16:55:13	57.29	38.19	5	5.6	3	67	0.49
20	2001/05/20	13:27:07	59.70	36.57	14	4.7	3	25	1.00
21	2003/04/16	11:06:05	57.56	30.03	10	4.4	4	40	1.65
22	2003/07/03	14:59:32	60.75	35.58	28	5.2	5	96	0.88
23	2003/12/26	01:56:56	58.36	29.08	5	6.6	27	78	0.16
24	2004/08/21	03:32:42	57.51	37.91	22	5.0	5	63	0.96
25	2004/10/06	11:14:37	57.94	28.77	10	5.2	6	46	0.69
26	2005/05/01	18:58:42	56.93	30.84	10	5.1	8	45	0.77
27	2005/05/14	18:04:54	56.91	30.74	10	5.2	12	91	0.86
28	2005/08/07	17:23:47	58.43	36.54	30	5.0	4	75	1.02
29	2006/02/18	11:03:36	55.85	30.74	16	4.6	7	66	1.55
30	2006/05/07	06:20:56	56.67	30.80	8	5.0	3	43	0.85
31	2006/09/16	10:42:52	57.69	37.38	5	4.9	5	103	1.27
32	2007/03/26	06:36:53	58.38	29.20	10	4.7	5	36	1.33

*Stress drop.
†Brune's corner frequency.

Atkinson, 1997; Atkinson and Cassidy, 2000; Siddiqqi and Atkinson, 2002; and Motazedian, 2006).

In equation (2), κ_0 characterizes the near-surface attenuation and is related to the kappa factor $\kappa = \kappa_0 + \kappa_r R$ (Anderson and Hough, 1984). Parameter κ for horizontal and vertical components were obtained from the slope of the smoothed log Fourier spectral amplitudes in the frequency band within which the spectral amplitudes start to decay exponentially and stop decreasing with frequencies due to background noise. The observed beginning frequency of the log–linear bands varies between 2 and 5 Hz depending on the event size and hypocentral distance. The distance-dependent κ for horizontal and vertical components are $\kappa_h = 0.048 + 0.0001R$ and $\kappa_v = 0.035 + 0.0001R$, respectively. A larger value of κ_{0h} compared with that of κ_{0v} confirms that the attenuation of higher frequencies is less on vertical components than on horizontal components. This implies that the vertical components are affected less by local site conditions. There are several estimates of κ_0 for various parts of the world. Boore and Joyner (1997) gave an estimate of $\kappa_0 = 0.035$ for generic rock sites in California. $\kappa_{0h} = 0.05$ and $\kappa_{0v} = 0.029$ were obtained by Motazedian (2006) for northern Iran, which is located immediately near the northwest of the study region. The most ambiguous part is the κ_0-value, which should be incorporated with the H/V ratio because both horizontal and vertical components have already gone through surface attenuations, but with different κ_0-values. Although it is assumed that the vertical amplification is negligible compared with the horizontal, considerable near-surface attenuation for vertical component is observed ($\kappa_{0v} = 0.029$ in this study). The common case is when κ_{0v} is not zero and is not identical to κ_{0h}. In this general case, a portion of κ_0-value ($\Delta\kappa_0 = \kappa_{0h} - \kappa_{0v}$) has already been included in the H/V ratio; thus, it should be subtracted from the near-surface attenuation term for the horizontal component. Hence, the site term for the horizontal component (Motazedian, 2006) can be considered as

$$S(f) = \mathrm{H/V} e^{-\pi(\kappa_{0h} - \Delta\kappa_0)f} = \mathrm{H/V} e^{-\pi\kappa_{0v} f}.$$

To calculate the H/V ratio, we tested several cases (e.g., averaging, linear, and quadratic regressions of ratios with

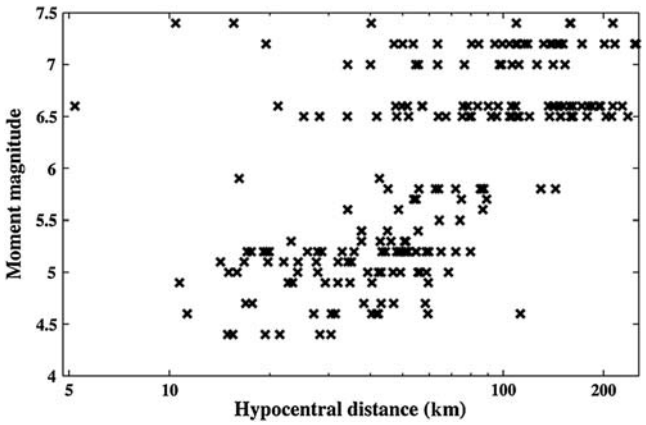

Figure 2. Distribution of the earthquake magnitudes versus hypocentral distances.

frequency). The results indicated that the case of averaging the H/V ratio taken over the whole frequency content would comparatively minimize the average residual errors for the source function that we are ultimately seeking for the earthquakes in the area. So site effect becomes

$$S_{ij}(f) = (\overline{\mathrm{H/V}})_{ij} e^{-\pi \kappa_{0v} f}, \tag{3}$$

in which $(\overline{\mathrm{H/V}})_{ij}$ is the average of H/V ratios of the earthquake i registered at station j. Table 2 lists the distribution of $(\overline{\mathrm{H/V}})_{ij}$ ratios among the records we used. Then the spectral amplitude A'_{ij} corrected for site effect becomes

$$\log A'_{ij} = \log A_{ij} - \log[(\overline{\mathrm{H/V}})_{ij} e^{-\pi f (0.035)}]. \tag{4}$$

Geometrical Spreading

Validity of assuming a simple shape for the attenuation curve, with a constant geometrical spreading b for both near-source and regional distances, is questionable. The wave-propagation studies indicate that the expected shape of amplitude decay for simple layered crustal models is complex (e.g., Burger *et al.*, 1987; Ou and Herrmann, 1990; Atkinson and Mereu, 1992). Layering in the crust causes direct-wave amplitudes to decay more steeply than R^{-1}. Then, as the direct arrivals are joined by postcritical reflection off the Moho and intracrustal discontinuities, there may be distance ranges over which amplitudes actually increase with distance, between approximately 50 and 200 km. Atkinson and Mereu (1992) have shown that the attenuation curve in southeastern Canada has three distinct sections. Their results indicate that at distances less than 70 km, corresponding to attenuation of the direct wave, amplitudes decay slightly more rapidly than $1/R$. Between 70 and 130 km, the amplitudes are approximately constant. Beyond 130 km, amplitude decays at a rate that is consistent with $R^{-0.5}$. Shoja-Taheri *et al.* (2007) have shown that the attenuation curve for use in determining the local magnitude M_L in eastern Iran has distinct sections of hinged trilinear form.

Table 2
Distribution of $\overline{\mathrm{H/V}}$ Ratios among the Records

$\overline{\mathrm{H/V}}$	Number of Records
1.00–1.49	27
1.50–1.99	65
2.00–2.49	93
2.50–2.99	35
3.00–3.49	14
3.50–3.99	6
4.00–4.50	3

Geometrical parameters represented by b in the attenuation relation show negligible variation with frequency (Atkinson and Mereu, 1992; Atkinson, 2004; Allen *et al.*, 2007). In addition, for frequencies less than 2.0 Hz and for distances shorter than 100 km, the anelastic coefficient is also negligible (Atkinson, 2004). Thus, we chose to examine the shape of the near-source attenuation by using only a subset of earthquakes which were recorded by at least three stations within 100 km from the hypocenters (there are 29 earthquakes which have this condition). As the first approximation (due to theoretical approach), it is assumed that the source spectrum of each subset events at low frequencies can be estimated by correcting observed spectra for geometric spreading by multiplying the distances R by $b = 1$. This is close to the b_1-value given for this region by Shoja-Taheri *et al.* (2007).

For observations within 100 km, the source spectrum of each earthquake at frequency 1.56 Hz can be estimated using equation (5) by averaging (log average) the site-corrected attenuation spectra over all stations that recorded the event (e.g., Atkinson, 2004). In this relation, A'_{ij} is the site-corrected amplitude spectrum of event i recorded at station j, N is the number of stations that recorded the event, f is the frequency (which is 1.56 Hz in this relation), and $\log A_{i0}(f)$ is the log of source spectrum:

$$\frac{1}{N}\sum_{j=1}^{N} \log A'_{ij}(f) R_{ij} \approx \log A_{i0}(f). \tag{5}$$

Subtracting equation (5) from equation (4) gives the normalized spectral amplitude $\log A_{nij}(f)$ as described in equation (6), which depends only on geometrical spreading and anelastic attenuation for $f < 2$ Hz:

$$\log A_{nij}(f) = \log A'_{ij}(f) - \frac{1}{N}\sum_{j=1}^{N} \log A'_{ij}(f) R_{ij} \approx -b \log R_{ij} - c_4(f) R_{ij}. \tag{6}$$

As shown in Figure 3, the rate of decay of $\log A_{nij}(f)$ varies with distance. At distances less than 80 km, the amplitude decays nearly constant. Between 80 and 120 km, the amplitudes are approximately constant. Beyond 120 km, the amplitudes also decay at a constant rate. To estimate the

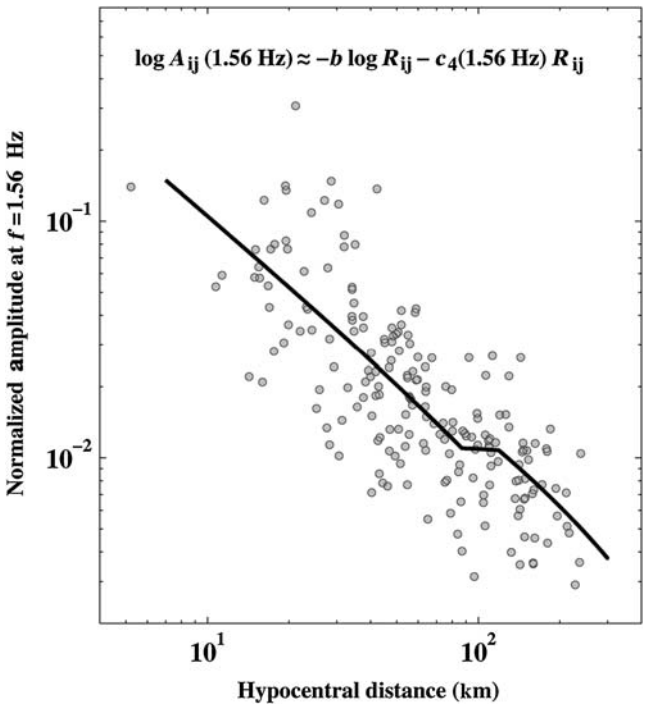

Figure 3. Decay rate of the normalized spectral amplitudes to a common source level $\log A_{nij}(f)$ versus distance.

attenuation parameters of b and $c_4(f)$ in equation (6), we allowed the parameter b to take separate values b_1, b_2, and b_3 in three different distance ranges using the hinged trilinear form of attenuation. We then applied the Monte Carlo simulation technique (Kalos and Whitlock, 2008) by generating random numbers confined within the predefined ranges (Table 3). We tested all possible combinations of the coefficients to search for the combination that minimizes the average residual errors. The best fits for the parameters that yield minimum mean of residual and minimum standard deviation are listed in Table 3.

Q Factor

The parameter $c_4(f)$ can be related to quality Q factor. According to Bakun and Joyner (1984), $Q(f)$ is given as

$$Q(f) = \pi f / c_4(f)\beta \ln 10, \tag{7}$$

in which the average S-wave crustal velocity $\beta = 3.5$ km/s is assumed. In order to estimate the Q factor for the S wave, we employ equation (8), in which A''_{ij} is the spectrum of event i at station j corrected for both geometrical spreading and site effects. While variation of geometrical parameters b with frequency is negligible, dependency of anelastic attenuation on frequency cannot be ignored. Therefore, $c_4(f)$ is evaluated by using the b-values that were estimated at the low frequency. So we have

$$\log A''_{ij}(f) = \log A'_{ij} + b \log R_{ij} = \log A_{i0}(f) - c_4(f) R_{ij}. \tag{8}$$

At a given frequency, events with the same moments lead to the same source spectrum $A_{i0}(f)$. Hence, for a given moment, $c_4(f)$ is simply equal to the slope of $\log(A''_{ij})$ versus R_{ij}. Applying $c_4(f)$ values in equation (7) gives the quality factor $Q(f)$ values. Figure 4 shows $Q(f)$ as a function of frequency. Fitting Q-values versus frequency with the form $Q = Q_0 f^{\alpha}$ (Aki, 1980) gives

$$Q(f) = (166^{+15}_{-13}) f^{(1.13 \pm 0.07)}. \tag{9}$$

Our estimate of Q-values generally agrees with the Q-values reported for different areas of eastern Iran and its vicinity. For northeastern Iran, $Q(1\text{ Hz}) \approx 160$ reported by Shoja-Taheri, *et al.* (2008). Ma'hood and Hamzeloo (2009) have estimated the coda quality factor, $Q_c = 104 f^{0.94}$ for the region of southeastern Iran. Nuttli (1980) showed that the attenuation of 1 s period crustal phases in Iran is relatively high, with an apparent Q-value of 150 for *Sn* and 125 for *Pg*.

Source Parameters

The source spectra $A_{i0}(f)$ in equation (8) can be written in terms of $Q(f)$ parameter as

$$A_{i0}(f) = A''_{ij}(f) e^{\frac{\pi f R_{ij}}{\beta Q(f)}}, \tag{10}$$

in which $A''_{ij}(f)$ is the amplitude spectrum corrected for site effect and geometrical spreading. The source spectra $A_{i0}(f)$ in equation (10) can now be evaluated using the $Q(f)$ values. We now compare the source spectrum $A_{i0}(f)$ with the Brune source model (Brune, 1970), which is generally employed for interpretation of earthquake source spectrum. The Brune point-source model simply relates the shear-wave radiation to the stress release across a circular fault rupture; its radius is related to the corner frequency. The high-frequency level of the source spectrum in the Brune model is controlled by the stress, whereas its low-frequency level is proportional to the seismic moment. Thus, the model interprets the observed spectra in terms of moment magnitude and stress drop. To

Table 3
Coefficients of Geometrical Spreading and Anelastic Decay Parameters

	R_1 (km)	R_2 (km)	b_1	b_2	b_3	c_4 (1.56 Hz)
Predefined	70–110	$-(R_1 + 60)R_1$	0.8–1.3	−0.3–0.3	0.4–1.0	(0.0–0.005)
Result	87 ± 2	119 ± 6	0.97 ± 0.080	-0.15 ± 0.10	0.73 ± 0.19	0.0009 ± 0.0003

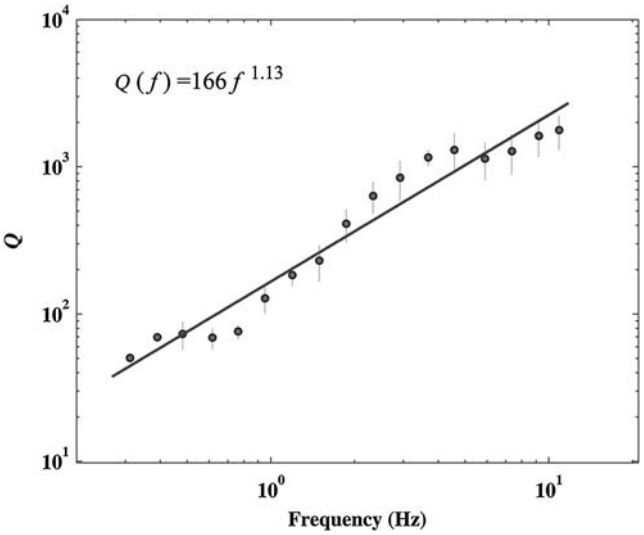

Figure 4. Quality factor $Q(f)$ as a function of frequency.

compare our source spectra with that of the Brune's model we should determine the stress drop and moment magnitude for each earthquake. The Brune's model acceleration spectrum is given by

$$A(f, M_0) = CM_0(2\pi f)^2/[1 + (f/f_0)^2]. \qquad (11)$$

Here, $f_0 = 4.9 \times 10^6 \beta(\sqrt[3]{\sigma/M_0})$; $C = FV\Re_{\theta p}/4\pi\rho\beta^3 R$, in which the crustal density ρ is equal to 2.7 g/cm^3, shear-wave velocity β is equal to 3.5 km/s, the average radiation pattern for shear waves $\Re_{\theta p}$ is equal to 0.55, the amplification of free surface F is equal to 2, the coefficient of energy partition onto two horizontal components V is equal to 0.7, R is distance in kilometers (assumed to be 1 km at source), $\Delta\sigma$ is Brune stress drop in bars, M_0 is seismic moment in dyne centimeters, and σ is the corner frequency in hertz. To determine M_0, σ, and f_0, we employed the method introduced by Andrews (1986). In this method, the source parameters can be evaluated by using the integrals of the squared velocity $I_V = 2\int_0^{+\infty} V^2(t)dt$ and squared displacement $I_D = 2\int_0^{+\infty} D^2(t)dt$ through the relations

$$f_0 = 1/2\pi\sqrt{I_V/I_D},$$
$$\sigma = \frac{2\rho}{1.28} I_V^{\frac{5}{4}} I_D^{-\frac{3}{4}}, \quad \text{and}$$
$$\Omega_0 = 2I_D^{3/4} I_V^{-1/4},$$

in which $\Omega_0 = CM_0$ is the low-frequency spectrum level of displacement according to Brune's ω^2 model (equation 11). To calculate the integrals of I_V and I_D for each record, we examined several time spans (including 50%, 75%, 95%, and 100% of the whole trace durations after the onset of S waves) and selected the time duration that gives the best correlation between the moment magnitude reported by the Global CMT catalog and that measured from the strong-motion data. The estimates of f_0 and $\Delta\sigma$ are listed in Table 1.

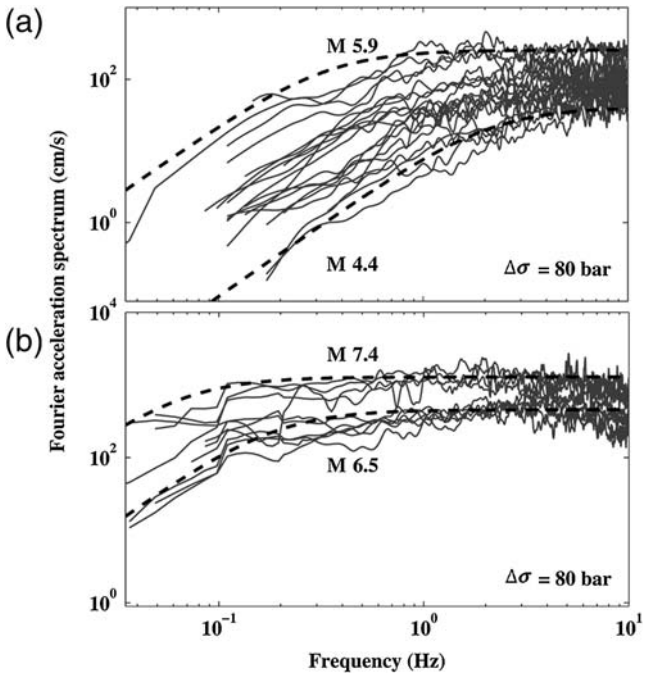

Figure 5. Acceleration source spectra $A_0(f, M_0)$ compared with the Brune (1970) model point-source spectrum plotted as a reference with stress drop of 80 bars for (a) **M** 4.4–5.9 and (b) **M** 6.5–7.4.

Mean value of $\Delta\sigma$ averaged over all events is 81 ± 36 bars. This is very close to the stress drop reported for California (Atkinson and Hanks, 1995) but is notably less than the stress drops reported for northeastern America (Atkinson and Boore, 2006; Boore *et al.*, 2010).

Figure 5 shows the acceleration source spectra $A_{i0}(f)$ for earthquakes with **M** 4.4–5.9 and **M** 6.5–7.4 (there is a gap between **M** 6.0–6.4 in our data) in comparison with the Brune point-source model, which is plotted for a reference stress drop of 80 bars.

Regardless of the large scatter in the observed stress drops (see Table 1), the Brune model shape in Figure 5a shows relatively good match with the source spectra for **M** 4.4–5.9. However, as observed in Figure 5b the spectra of larger events, which are generally associated with finite and extended fault ruptures, do not match with those of the Brune point-source model at low- to midfrequencies. So, we will view, in more quantitative details, the possible departure of the spectral shape of the events from that of Brune's model.

Construction of an Empirical Source Model

Departure of medium to large earthquake spectra from the simple Brune model is expected to be based upon models that would give rise to more than one corner frequency in the spectrum. These models include a rectangular (as opposed to circular) fault rupture (Haskell, 1969; Savage, 1972), the Brune (1970) partial stress-drop model, and raggedness of

Table 4
Functional Form of Earthquake Amplitude Source Spectrum

Model	$A_0(f, M_0)$
AB95 ($\mathbf{M} \geq 4$)*	$CM_0(2\pi f)^2\{(1-\varepsilon)/[1+(f/f_a)^2] + \varepsilon/[1+(f/f_b)^2]\}$
AS97†	$CM_0(2\pi f)^2/\{(1-\varepsilon)/[1+(f/f_a)^2] + \varepsilon/[1+(f/f_b)^2]\}$
J97‡	$CM_0(2\pi f)^2/\{[1+(f/f_a)^2]^{0.75}[1+(f/f_b)^2]^{0.25}\}$
This study	$CM_0(2\pi f)^2/\{[1+(f/f_a)^2]^{\varepsilon}[1+(f/f_b)^2]^{1-\varepsilon}\}$

*Atkinson and Boore (1995) for northeastern America.
†Atkinson and Silva (1997) for California.
‡Joyner (1997) for northeastern America and southeastern Canada.

Table 5
Magnitude-Dependent Corner Frequencies of f_a and f_b and Parameters ε

Model	$\log(f_a)$	$\log(f_b)$	$\log(\varepsilon)$
AB95 ($\mathbf{M} \geq 4$)*	2.410–0.533M	1.430–0.188M	2.520–0.637M
AS97†	2.181–0.496M	1.778–0.302M	2.764–0.623M
J97‡	2.312–0.500M	3.609–0.500M	–
This study	2.69–0.56M	3.40–0.53M	0.10–0.03M

*Atkinson and Boore (1995) for northeastern America.
†Atkinson and Silva (1997) for California.
‡Joyner (1997) for northeastern America and southeastern Canada.

fault surface interpreted as the asperity model (Hartzell and Brune, 1979; McGarr, 1981), the barrier model (Papageorgiou and Aki, 1983), and multiple-event models (Joyner and Boore, 1986; Boatwright, 1988). As listed in Tables 4 and 5, some models of source spectra with two corner frequencies have been suggested for earthquakes in California and eastern North America (Atkinson and Boore, 1995; Atkinson and Silva, 1997; Joyner, 1997). To construct an empirical two-corner-frequency source model for earthquake source spectra in eastern Iran (horizontal component of the shear-wave spectrum), for $\mathbf{M}$ 4.4–7.4, we tested several functional forms (including those suggested for California and eastern North America) by employing the Monte Carlo simulation technique (Kalos and Whitlock, 2008) to our ground-motion database to search for the best combination of the coefficients that minimizes the average residual errors. The earthquake source spectrum we attained for horizontal components of ground motion is given by a functional form that represents the multiplication of two Brune spectra with corner frequencies of f_a and f_b, and a parameter ε given as

$$A_0(f, M_0) = CM_0(2\pi f)^2/\{[1+(f/f_a)^2]^{\varepsilon}[1+(f/f_b)^2]^{1-\varepsilon}\}, \quad (12)$$

in which f_a, f_b, and ε as functions of magnitude are

$$\log(f_a) = 2.69 - 0.56\mathbf{M}, \quad (13)$$

$$\log(f_b) = 3.40 - 0.53\mathbf{M}, \quad (14)$$

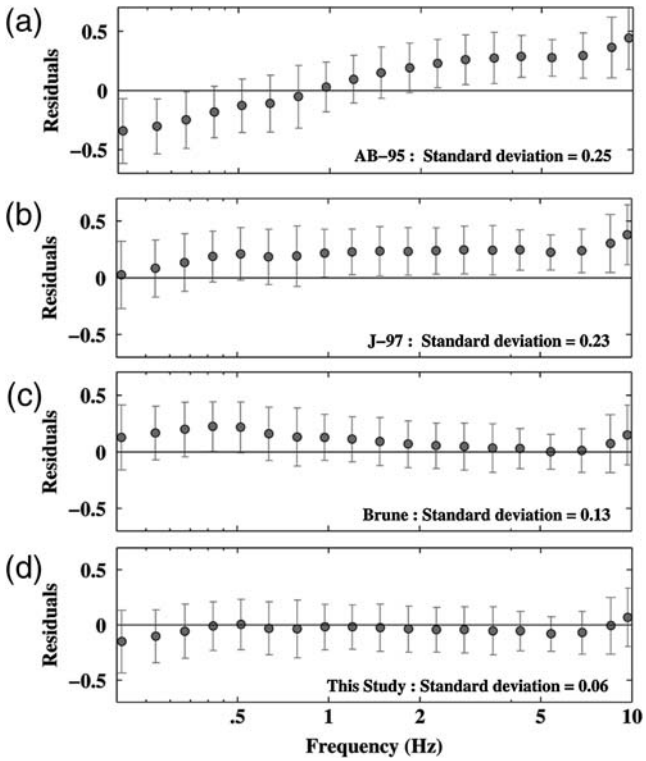

Figure 6. Variation of the residuals, defined as log(pred.) − log(obs.), of source functions for four models as a function of frequency for $\mathbf{M} > 6.0$: (a) Atkinson and Boore (1995); (b) Joyner (1997); (c) Brune (1970); and (d) model proposed in this study.

and

$$\log(\varepsilon) = 0.10 - 0.03\mathbf{M}. \quad (15)$$

Comparing the functional form of our model with those reported for earthquakes in California and eastern North America (Table 4) shows that the source spectrum we developed (equation 12) is similar to the functional form of the Joyner (1997) model, with the exception that the parameter ε in our model is magnitude dependent, whereas in the Joyner model this parameter was assigned a constant value of 0.75.

To measure how well our model fits the datasets, the resulting mean residuals are plotted as function of frequency in Figure 6 for $\mathbf{M} > 6.0$ and compared with the residuals corresponding to other model shapes (e.g. Brune, 1970; Atkinson and Boore, 1995; and Joyner, 1997). The Atkinson and Boore (1995) and Joyner (1997) models both show serious mismatch with our dataset (see Fig. 6a and 6b, respectively). Figure 6c shows that while Brune's model agrees rather well with the observed spectra within f = 2–9 Hz, it overestimates notably the spectra within the low- to midfrequencies. On the other hand, our proposed model (equations 12–15) resembles the source spectral amplitudes well enough within a wide range of frequencies between 0.05 and 10 Hz (Fig. 6d) that it can therefore represent the shape of source spectrum of

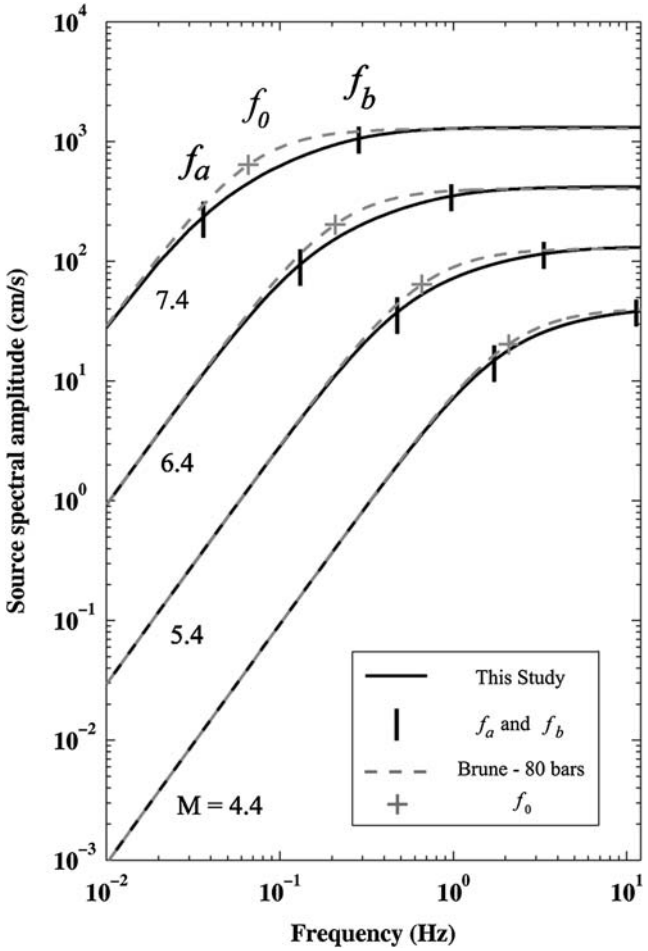

Figure 7. The proposed two-corner model for eastern Iran source spectral amplitude ($R = 1$ km, horizontal component) as a function of frequency. The solid curves are for **M** 4.4, 5.4, 6.4, and 7.4. Vertical bars show the target corner frequencies of f_a and f_b. The dashed curves show the Brune model point-source spectra plotted as a reference with stress drop of 80 bars. The plus symbols show the locations of Brune's corner frequencies.

earthquakes in the eastern Iran region within the limits of observed errors.

In Figure 7, shapes of source spectral amplitude ($R = 1$ km, horizontal component) for events of magnitudes **M** 4.4–7.4, are compared with the Brune model point-source spectrum as a reference with stress drops of 80 bars. Because of gradually increasing complexity of source mechanics with increasing events magnitude, the observed spectral sags at intermediate frequencies, relative to the Brune model, become more prominent with increase of magnitude. Amplitude reduction of our model with respect to Brune's model averaged between the corner frequencies of f_a and f_b shows increasing growth from 4% at **M** 4.4 to 30% at **M** 7.4. Equation (12) is the simplest functional form that matches spectral amplitudes and corner frequencies. It is an empirical representation rather than theoretical model. The reduction of spectral amplitudes at intermediate frequencies relative to Brune's model has an important implication for seismic

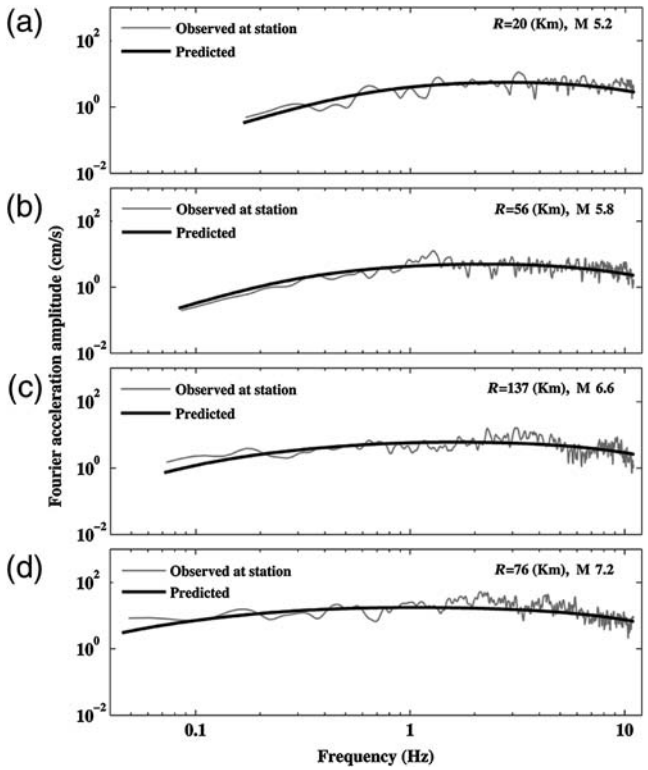

Figure 8. Predicted amplitude spectra $A(f, M_0, R)$ are compared with the observed spectrum for (a) $R = 20$ km, **M** 5.2; (b) $R = 56$ km, **M** 5.8; (c) $R = 137$ km, **M** 6.6; and (d) $R = 76$ km, **M** 7.2.

hazards and building codes. For events of **M** ≤4.4 the shape of the model approaches that of Brune's model.

Prediction of Amplitude Spectrum $A(f, M_0, R)$ at Distance R from a Source

We are now able to simulate the amplitude spectrum $A(f, M_0, R)$ for a given moment magnitude at a distance R with site effect $S(f)$ by combining the source spectral shape $A_0(f, M_0)$, with the geometrical spreading coefficients listed in Table 3 and the anelastic decay parameters, $Q(f)$, given by equation (9). In Figure 8, the predicted spectra are compared with the corresponding spectra of four events of **M** 5.2, 5.6, 6.2, and 7.2 which were recorded, respectively, at four hypocentral distances of $R = 20$, 56, 141, and 76 km. As shown, there are generally good agreements between the observed and predicted spectra. This indicates that the source spectral function proposed in equation (12) can be used reliably in constructing the amplitude spectra of earthquakes in the region when it is incorporated with the path and site parameters evaluated in the present study.

Figure 9 also displays an example in which the residuals and their means between the observed and predicted amplitude spectra of events are displayed as functions of distance R for three separate frequencies of 2, 5, and 8 Hz. The good agreement between the results of the model and observations

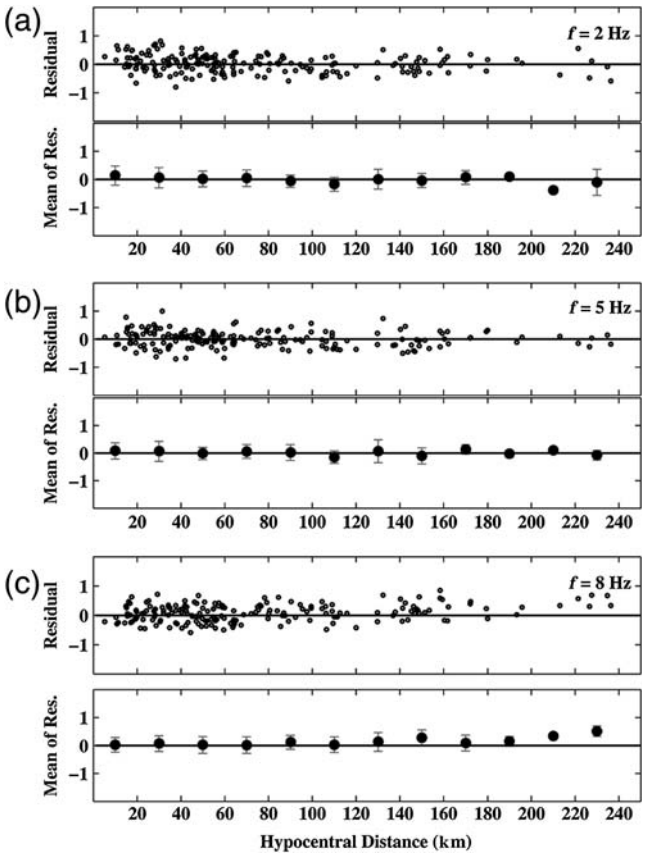

Figure 9. Estimate of residuals, defined as log(pred.) − log(obs.), of the amplitude spectra of all records as a function of distance for (a) $f = 2$ Hz, (b) $f = 5$ Hz, and (c) $f = 8$ Hz. Estimates of residual means are also depicted at several distance ranges centered at the filled circles.

is convincing in that the model can reliably predict the amplitude spectrum $A(f, M_0, R)$ for the wide ranges of frequency, magnitude, and hypocentral distance R used in this study.

Conclusions

Acceleration time series of 32 earthquakes recorded on Building and Housing Research Center strong-motion stations were processed and analyzed to obtain region-specific key seismic parameters and source spectral shape for earthquakes in eastern Iran. Fourier amplitude spectra were used to determine a geometric spreading model and anelastic attenuation by using the Monte Carlo simulation technique. A trilinear geometric spreading model is suggested with hinges at 87 and 119 km. The regional Q-value is $Q(f) = 166f^{1.13}$, based on the obtained trilinear geometric spreading model for the region. The kappa factors, for both horizontal and vertical components, were obtained from the slope of the smoothed amplitude of Fourier acceleration spectrum at higher frequencies. Horizontal and vertical components of κ_0 are 0.048 and 0.035, respectively. The clear difference between vertical and horizontal suggests that there should be a distinguishable near-surface site-attenuation effect on the horizontal components compared with the vertical component. In the absence of adequate information of soil classification for the ISMN stations used in this study the H/V spectral ratio was, alternatively, used as a rough estimate of site amplification. The overall site term, which is the site amplification multiplied by the near-surface attenuation, is obtained by $(\mathrm{H/V})e^{-\pi\kappa_{0v}}$, as described by Motazedian (2006). The Brune point-source modeling suggests average stress drop 81 ± 36 bars. This is very close to the stress drop reported for California (Atkinson and Hanks, 1995) but is noticeably less than those reported for northeastern America (Atkinson and Boore, 2006; Boore *et al.*, 2010). To construct an empirical model shape for eastern Iran source spectra (horizontal component of the shear-wave spectrum), several functional forms were tested, including those suggested for California and northeastern America (Atkinson and Boore, 1995; Atkinson and Silva, 1997; and Joyner, 1997). As presented by equation (12), the model we attained is a function of the two multiplicative corner frequencies of f_a and f_b and parameter ε, in which f_a, f_b, and ε are magnitude dependent. The model shows good match with the source spectra of events in the frequency range used in the regression. Comparison made between the source spectral shape and the Brune point-source model indicates that while there are good matches between the models at low- and high-frequency levels, our model shape undergoes a gradually increasing amplitude reduction with increase of magnitude. The observed sags of the proposed model with respect to the Brune model point source at intermediate frequencies are expected because source behavior becomes gradually more complex as the event's magnitude becomes larger. Amplitude reduction of the model, averaged between the two corner frequencies f_a and f_b with respect to the Brune model shows increasing growth from 4% at **M** 4.4 to 30% at **M** 7.4. The reduction of spectral amplitudes at intermediate frequencies has important implications for seismic hazards and building codes. Employing the results of wave-propagation parameters to the model shape spectra makes it possible to simulate the amplitude spectrum of earthquakes within the range of frequencies, magnitudes, and hypocentral distances used in this study.

Data and Resources

Strong ground motion data used in this study were obtained from Iran Strong Motion Network; Building and Housing Research Center, Ministry of Housing & Urban Development (www.bhrc.gov.ir/; last accessed April 2010). The assigned moment magnitude (**M**) for the events with **M** ≥5.0 is that reported by the Global Centroid Moment Tensor catalog (www.globalcmt.org/; last accessed April 2010).

Acknowledgments

Ground-motion data were obtained from the Iran Strong Motion Network. We would like to thank Saeid Naserih and Hadi Ghofrani for their

thoughtful reviews. We also thank Associate Editor Arthur McGarr and two anonymous reviewers for their constructive comments.

References

Aki, K. (1980). Attenuation of shear waves in the lithosphere for frequencies from 0.5 to 25 Hz, *Phys. Earth Planet. In.* **74,** 615–631.

Allen, T. I., T. Dhu, P. R. Cummins, and J. F. Schneider (2007). Attenuation of ground-motion spectral amplitudes in southeastern Australia, *Bull. Seismol. Soc. Am.* **97,** 1279–1292.

Anderson, J. G., and S. Hough (1984). A model for the shape of the Fourier amplitude spectrum of acceleration at high frequencies, *Bull. Seismol. Soc. Am.* **74,** 1969–1993.

Andrews, D. J. (1986). Objective determination of source parameters and similarity of earthquakes of different size, in *Earthquake Source Mechanics*, S. Das, J. Boatwright, and C. H. Scholz (Editors), American Geophysical Union, Washington, D.C., 259–267.

Atkinson, G. M. (1989). Attenuation of the *Lg* phase and site response for the Eastern Canada Telemetered Network, *Seismol. Res. Lett.* **60,** 59–69.

Atkinson, G. M. (1993). Earthquake source spectra for earthquakes in eastern North America, *Bull. Seismol. Soc. Am.* **83,** 1778–1798.

Atkinson, G. M. (2004). Empirical attenuation of ground-motion spectral amplitudes in southeastern Canada and the northeastern United States, *Bull. Seismol. Soc. Am.* **94,** 1079–1095.

Atkinson, G. M., and D. Boore (1995). Ground-motion relations for eastern North America, *Bull. Seismol. Soc. Am.* **85,** 17–30.

Atkinson, G. M., and D. M. Boore (2006). Earthquake ground-motion prediction equations for eastern North America, *Bull. Seismol. Soc. Am.* **96,** 2181–2205.

Atkinson, G. M., and J. F. Cassidy (2000). Integrated use of seismograph and strong-motion data to determine soil amplification: Response of the Fraser River delta to the Duvall strait and Georgia strait earthquakes, *Seismol. Soc. Am.* **90,** 1023–1040.

Atkinson, G. M., and T. C. Hanks (1995). A high-frequency magnitude scale, *Bull. Seismol. Soc. Am.* **85,** 825–833.

Atkinson, G. M., and R. F. Mereu (1992). The shape of ground motion attenuation curves in southeastern Canada, *Bull. Seismol. Soc. Am.* **82,** 2014–2031.

Atkinson, G. M., and W. Silva (1997). An empirical study of earthquake source spectra for California earthquakes, *Bull. Seismol. Soc. Am.* **87,** 97–113.

Bakun, W. H., and W. B. Joyner (1984). The M_L scale in central California, *Bull. Seismol. Soc. Am.* **74,** 1827–1843.

Beresnev, I. A., and G. M. Atkinson (1997). Modeling finite-fault radiation from the ω^n spectrum, *Seismol. Soc. Am.* **87,** 67–84.

Boatwright, J. (1988). The seismic radiation from composite models of faulting, *Bull. Seismol. Soc. Am.* **78,** 489–508.

Boatwright, J., and G. L. Choy (1992). Acceleration source spectra anticipated for large earthquakes in northeastern America, *Bull. Seismol. Soc. Am.* **82,** 660–682.

Boore, D. M. (2003). Simulation of ground motion using the stochastic method, *Pure Appl. Geophys.* **169,** 635–676.

Boore, D. M., and W. B. Joyner (1997). Site amplifications for generic rock sites, *Bull. Seismol. Soc. Am.* **87,** 327–341.

Boore, D. M., K. W. Campbell, and G. M. Atkinson (2010). Determination of stress parameters for eight well-recorded earthquakes in eastern North America, *Bull. Seismol. Soc. Am.* **100,** 1632–1645.

Brune, J. N. (1970). Tectonics stress and the spectra of seismic shear waves from earthquakes, *J. McGuire Geophys. Res.* **75,** 4997–5009.

Burger, R., P. Somerville, J. Barker, R. Herrmann, and D. Helmberger (1987). The effect of crustal structure on strong ground motion attenuation relations in eastern North America, *Bull. Seismol. Soc. Am.* **77,** 420–439.

Haddon, R. (1996). Earthquake source spectra in eastern North America, *Bull. Seismol. Soc. Am.* **86,** 1300–1313.

Hartzell, S., and J. Brune (1979). The Horse Canyon earthquake of August 2, 1975-two-stage stress-release process in strike slip earthquake, *Bull. Seismol. Soc. Am.* **69,** 1161–1178.

Haskell, N. (1969). Elastic displacements in the near-field of propagating fault, *Bull. Seismol. Soc. Am.* **59,** 865–908.

Joyner, W. (1997). Ground motion estimates for the northeastern U.S. or southeastern Canada, in *Recommendations for Probabilistic Seismic Hazard Analysis: Guidance on Uncertainty and Use of Experts*, Senior Seismic Hazard Analysis Committee (R. Budnitz, G. Apostolakis, D. Boore, L. Cluff, K.Coppersmith, A. Cornell, and P. Morris), *U.S. Nuclear Reg. Comm. Rept. NUREG/CR-6372*, Washington, D.C.

Joyner, W., and D. Boore (1986). On simulating large earthquakes by Green's function addition of smaller earthquakes, in *Earthquake Source Mechanics, Maurice Ewing 6*, American Geophysical Union, Monograph, Vol. 37, 269–274.

Kalos, M. H., and P. A. Whitlock (2008). *Monte Carlo Method*, 2nd ed., Wiley, New York, 215 pp.

Lermo, J., and F. J. Chávez-García (1993). Site effect evaluation using spectral ratios with only one station, *Bull. Seismol. Soc. Am.* **83,** 1574–1594.

Ma'hood, M., and H. Hamzeloo (2009). Estimation of coda wave attenuation in east central Iran, *J. Seismol.* **13,** 125–139.

McGarr, A. (1981). Analysis of peak ground motion in terms of a model of inhomogeneous faulting, *J. Geophys. Res.* **86,** 3901–3912.

Motazedian, D. (2006). Region-specific key seismic parameters for earthquakes in northern Iran, *Bull. Seismol. Soc. Am.* **96,** 1383–1395.

Nakamura, Y. (1989). A method for dynamic characteristics estimation of subsurface using microtremor on the ground surface, *Q. Rep. Railway Tech. Res. Inst.* **30,** 25–33.

Nuttli, O. W. (1980). The excitation and attenuation of seismic crustal phases in Iran, *Bull. Seismol. Soc. Am.* **70,** 469–485.

Ou, G., and R. Herrmann (1990). A statistical model for peak ground motion from local to regional distances, *Bull. Seismol. Soc. Am.* **80,** 1397–1417.

Papageorgiou, A., and K. Aki (1983). A specific barrier model for quantitative description of inhomogeneous faulting and the prediction of strong motion, part I: Description of the model, *Bull. Seismol. Soc. Am.* **73,** 693–722.

Savage, J. (1972). Relation of corner frequency to fault dimensions, *J. Geophys. Res.* **97,** 3788–3795.

Shoja-Taheri, J., and M. Niazi (1981). Seismicity of the Iranian plateau and bordering regions, *Bull. Seismol. Soc. Am.* **71,** 477–489.

Shoja-Taheri, J., S. Naserieh, and A. H. Ghafoorian-Nasab (2008). An M_L scale in northeastern Iran, *Bull. Seismol. Soc. Am.* **98,** 1975–1982.

Shoja-Taheri, J., S. Naserieh, and H. Ghofrani (2007). M_L and M_w scales in the Iranian plateau based on the strong-motion records, *Bull. Seismol. Soc. Am.* **97,** 661–669.

Siddiqqi, J., and G. M. Atkinson (2002). Ground-motion amplification at rock sites across Canada as determined from horizontal-to-vertical component ratio, *Seismol. Soc. Am.* **92,** 877–884.

Stöcklin, J. (1968). Structural history and tectonics of Iran: A review, *Bull. Am. Assoc. Petrol. Geol.* **52,** 1229–1258.

Tchalenko, J. S. (1975). Seismicity and structure of Kopek Dagh (Iran, U.S.S.R.), *Phil. Trans. Roy. Soc. London* **278,** no. 1275, 1–25.

Woodgold, C. (1990). Estimation of *Q* in eastern Canada using coda waves, *Bull. Seismol. Soc. Am.* **80,** 411–429.

Earthquake Research Center (EQRC)
Ferdowsi University of Mashad
Machad, Iran

Manuscript received 28 January 2013;
Published Online 4 March 2014